



# 1 **Comparison of influence between two types of cold surge** 2 **on haze dispersion in Eastern China**

3 Shiyue Zhang<sup>1</sup>, Gang Zeng<sup>1</sup>, Xiaoye Yang<sup>1</sup>, Ruixi Wu<sup>2</sup>, Zhicong Yin<sup>1,3</sup>

4 <sup>1</sup> Key Laboratory of Meteorological Disaster of Ministry of Education (KLME),  
5 Collaborative Innovation Center on Forecast and Evaluation of Meteorological Disasters (CIC-FEMD),  
6 Nanjing University of Information Science and Technology, Nanjing, 210044, China

7 <sup>2</sup> Meteorological Bureau of Jiading District, Shanghai 201815, China

8 <sup>3</sup> Southern Marine Science and Engineering Guangdong Laboratory (Zhuhai), Zhuhai, 519080, China

9 *Correspondence to:* Gang Zeng ([zenggang@nuist.edu.cn](mailto:zenggang@nuist.edu.cn))

10 **Abstract.** Cold surge (CS) is considered as a favorable weather process to improve air quality and is  
11 widely recognized. However, there is no detailed study on the differences in the dispersion ability of  
12 different types of CSs to haze days in eastern China (HD<sub>EC</sub>). This paper uses the hierarchical clustering  
13 algorithm to classify the cool season (November to February of the following year) CSs across eastern  
14 China into blocking CSs and wave-train CSs and compares their influences on the number of HD<sub>EC</sub> from  
15 1980 to 2017. Results show that the wave-train CSs can significantly improve the visibility in eastern  
16 China and generally make the high air quality last for about 2 days longer than the blocking CSs, which  
17 indicates that the blocking CSs have a weaker ability to dissipate HD<sub>EC</sub> compared with the wave-train  
18 CSs. The CSs affect the HD<sub>EC</sub> by changing these meteorological elements like thermal inversion potential,  
19 horizontal surface wind, sea level pressure (SLP), and surface air temperature (SAT). 4 days after the  
20 CSs outbreak, the variations of thermal inversion potential and horizontal surface wind of two types of  
21 CSs tend to be consistent. However, the negative SAT anomalies, and the positive SLP anomalies caused  
22 by the blocking CSs lasted shorter than those caused by the wave-train CSs, which forms favorable  
23 conditions for the rapid growth of HD<sub>EC</sub>. Furthermore, results show that in recent years, especially after  
24 the 1990s, the frequency of wave-train CSs has decreased significantly, while the frequency of blocking  
25 CSs has slightly increased, indicating that the overall ability of CSs to dissipate HD<sub>EC</sub> has weakened in  
26 general.  
27



## 28 1. Introduction

29 Haze can reduce visibility and affect traffic and ecological sustainability (Xu et al., 2013; Xie et al.,  
30 2014; Wang et al., 2016). Studies have shown that the haze in China is mainly concentrated in the eastern  
31 region of China (EC), and its peak is noticeable in winter and spring (Wang et al., 2015, 2016). During  
32 haze days, the concentration of aerosol particles increases and results in a wide range of visibility decline  
33 (Luo et al., 2001; Xu, 2001; Wu et al., 2012; Fu et al., 2013; Wu et al., 2014). For example, in the winter  
34 of 2015, severe haze in the Beijing-Tianjin-Hebei region affected more than 500,000 square kilometers,  
35 causing heavy pollution in 37 cities (Chang et al., 2016; Zhang et al., 2016). After this event, researchers  
36 and policymakers paid more attention to the studies related to haze events. Besides, strict control  
37 measures of air pollution and energy emissions have also been put in place.

38 Many studies indicated that the long-term trends of haze are closely related to fossil-fuel emissions  
39 (Shi et al., 2008; Wei et al., 2017). On the other hand, meteorological conditions also play an important  
40 role in determining regional air quality. In addition to the influence of human activities, the formation of  
41 haze is closely related to static and calm weather conditions, such as strong thermal inversion potential  
42 (TIP), negative sea level pressure (SLP) anomaly, and weak wind speed (Niu et al., 2010; Cai et al.,  
43 2017). In recent years, due to the decreased relative humidity, it is difficult for haze particles to transform  
44 into fog drops, making the number of haze days present a rising trend (Ding and Liu, 2014). In addition,  
45 the anomalies of atmospheric circulation caused by global warming may also enhance the stability of the  
46 lower atmosphere, which leads to more severe and frequent haze pollution (Cai et al., 2017). All these  
47 emphasize that the threat of haze to human society could be more serious in the near future.

48 Global warming leads to the decrease of cold days and cold surges (CSs) by raising the surface air  
49 temperature (SAT), which also provides favorable conditions for the increase of haze days (Lin et al.,  
50 2009). CS is a typical extreme weather process in East Asia, which significantly impacts the atmospheric  
51 circulation to improve the local air quality (Hu et al., 2000; Qu et al., 2015; Wang et al., 2016). With the  
52 outbreak of CSs, a series of abrupt variations of meteorological elements such as the positive SLP  
53 anomaly, the decrease of SAT, and the enhancement of north wind component will occur in the areas  
54 where the CSs pass (CCiM et al., 1999). When a CS occurs, the arrival of fresh and dry cold air can  
55 dissipate and reduce local air pollutants (Lin et al., 2008). Wang et al. (2016) proposed that the " early in  
56 the north and late in the south " feature of air quality improvement in mainland China results from the



57 cold air masses moving southward from high latitudes to low latitudes after the outbreak of CSs.  
58 Although some studies have shown that the weakening of East Asian Winter Monsoon and global  
59 warming leads to the decrease of CSs (Qu et al., 2015; Wang et al., 2006), extreme low-temperature  
60 events are still frequent (Park et al., 2011a), which makes the assessment of haze dispersion capacity of  
61 cold air activities still full of uncertainty.

62 Previous studies have shown that the outbreak of CSs has an obvious effect on haze dispersion (Lin  
63 et al., 2009; Hien et al., 2011; Ashfold et al., 2017). However, most of them analyzed the haze variation  
64 during the CSs based on case analyses or considering the interannual influence of CS frequency on haze.  
65 Studies have shown that there are large differences between individual cases of CSs in terms of  
66 circulation anomalies, influence path and range (Park et al., 2014; Cai et al., 2019). Therefore, it is  
67 necessary to consider the influence of classified CSs on haze. Based on this limitation, the following two  
68 questions are proposed in this paper: Are there different effects of CSs' types on the haze days in EC  
69 ( $HD_{EC}$ )? If so, what is the physical mechanism that makes the difference? The solution to these issues  
70 will help us understand the mechanism of CSs in dissipating the haze and improving its predictability in  
71 the future.

72 The rest of this paper is organized as follows: Section 2 introduces the data and methods, while  
73 section 3 presents the study findings. The variation of  $HD_{EC}$  and its relationship with two types of CSs  
74 are shown in section 3.1. Section 3.2 explains the reason why different types of CSs have different  
75 abilities to dissipate  $HD_{EC}$ . The main conclusions and discussion are presented in section 4.

## 76 **2. Data and Methods**

### 77 **2.1 Data**

78 The datasets employed in this study were: (1) daily ERA-Interim atmospheric fields including SLP,  
79 air temperature at different levels, SAT, horizontal wind, and geopotential height (GPH) provided by the  
80 European Center for Medium-Range Weather Forecasts (ECMWF) (Dee et al., 2011). They have a  
81 horizontal resolution of  $1.0^{\circ} \times 1.0^{\circ}$ . (2) daily observational datasets for 756 meteorological stations from  
82 1980 to 2017 collected by the National Meteorological Information Center of China Meteorological  
83 Administration, including relative humidity, visibility, and weather phenomena. These datasets were  
84 observed four times per day (02:00, 08:00, 14:00, and 20:00LT). Stations with more than 5% missing

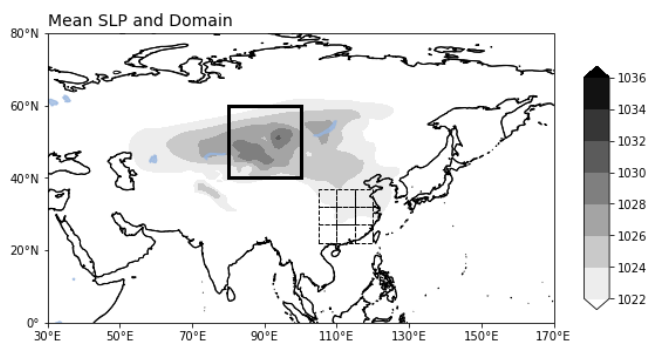


85 data were eliminated, while sporadic missing data were filled by cubic spline interpolation. Successive  
86 missing data were discarded.

## 87 2.2 Methods

88 The visibility and relative humidity (Rhum) are routinely used in meteorology to distinguish the  
89 haze (Yin et al., 2017). After filtering the other weather parameters affecting visibility (i.e., dust,  
90 precipitation, sandstorm), we defined a haze day as a day with visibility lower than 10 km and the Rhum  
91 less than 90 % occurring at any of the four times (02:00, 08:00, 14:00, and 20:00LT) (Yin et al., 2019a).  
92 Figure S1 shows the climatology of haze days in China from 1980 to 2017. The haze days are mainly  
93 concentrated in the EC (22°N-37°N, 106°E-121°E), which is selected as the target area in the present  
94 study. The monthly average of HD<sub>EC</sub> indicated that the HD<sub>EC</sub> mainly peaks (Figure S1b) in the cool  
95 season (November to February of the following year (NDJF)). Consequently, we chose cool season as  
96 the study period for HD<sub>EC</sub> in this research.

97 The CS is a cooling process superimposed on a cold day (Park et al., 2011a). The outbreak of the  
98 CSs in East Asia is closely related to the Siberian high, known as the Siberian high surge (Compo et al.,  
99 1999). In this study, we first divided EC into 5°×5° grid boxes as shown in Figure 1 and then calculated  
100 the average SAT for each box to avoid the extreme SAT anomaly in a single grid. To explore the impact  
101 of CSs on HD<sub>EC</sub>, the selection of CS in this paper fulfil the following three criteria (Park et al., 2011b) :  
102 (1) the maximum pressure center in the domain of the Siberian high (Figure 1) should exceed 1,035 hPa  
103 on the day of the CS outbreak. (2) the daily temperature drop ( $SAT_t - SAT_{t-1}$ ) and the SAT anomalies  
104 should exceed -1.5 standard deviation ( i.e., the standard deviation of the SAT from 1980 to 2017) at  
105 least one box. (3) the haze day appeared in the box where the CS occurs from -2 days to 0 day related to  
106 the occurred CS. A total of 187 CSs were identified in this paper.



107

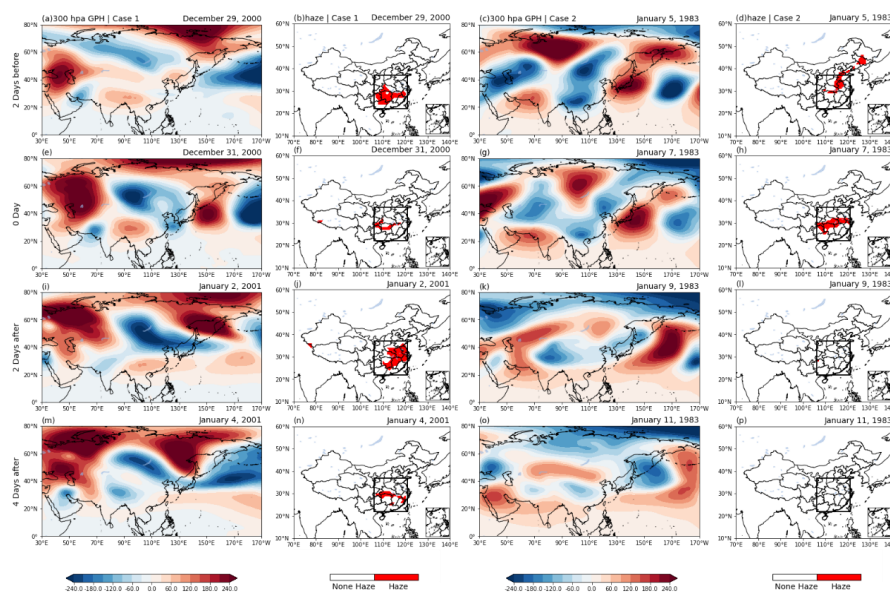
108 **Figure 1.** The domain of Siberian high (thick solid box; 40°N–60°N, 80°E–100°E) and EC (dotted box; 22°N–37°N,  
109 106°E–121°E) divided into 5°×5° grid boxes. Shadings indicate the cool season mean SLP.

110

### 111 3. Results

#### 112 3.1 The influence of two types of CSs on HD<sub>EC</sub>

113 The circulation evolution with different types of CSs is quite different (Park et al., 2013), which  
114 leads to the different distribution of surface meteorological conditions and haze. Here we display the  
115 evolutions of two typical CS events (Figure 2). These two events were selected because they belong to  
116 different types of CSs, referring to Park et al. (2008 and 2014), and have a large different effect on HD<sub>EC</sub>.  
117 Figures 2a, 2e, 2i, 2m show a CS that occurred on December 31, 2000, with positive and negative GPH  
118 anomalies over the sub-arctic and East Asian coast, respectively, which meet the definition of the  
119 blocking CS (Park et al., 2015). The blocking structure has a relatively stable lifecycle, so the HD<sub>EC</sub> only  
120 has a certain dispersion on the day of the CS outbreak, and heavy HD<sub>EC</sub> begins to emerge 2 days after  
121 the CS outbreaks (Figures 2j and 2n). Figures 2c, 2g, 2k, 2o indicate a CS that occurred on January 7,  
122 1983, which meets the definition of the wave-train CS (Chai et al., 2002; Park et al., 2015). The CS is  
123 associated with the wave-train structure of “-+ - +” at the upper troposphere. The cold air moves from  
124 west to east and invades EC along with this zonal wave-train (Yang et al., 2020a). The wave-train CS has  
125 a better ability to disperse HD<sub>EC</sub>, and there is no new HD<sub>EC</sub> appear for a long time after the wave-train  
126 CS erupts (Figures 2l and 2p).



127

128 **Figure 2.** Composite of GPH anomalies (shading: gpm) at 300 hPa from -2 days to 4 days for case1 CS outbreak on  
 129 December 31, 2000 (a, e, i, m), and case2 CS outbreak on January 7, 1983 (c, g, k, o), and the related spatial  
 130 distribution of HD<sub>EC</sub> (shading) (b, f, j, n and d, h, l, p).

131

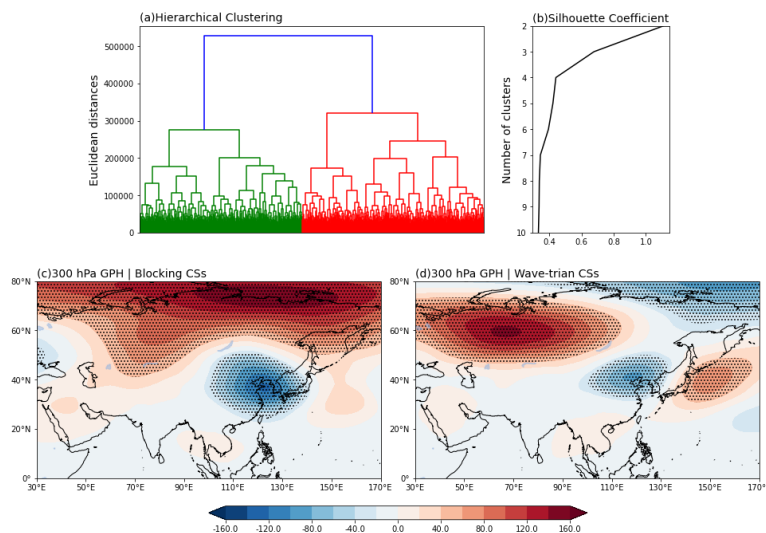
132 The case analysis results indicate that the ability of different types of CSs to haze dispersion is  
 133 different. Referring to the research of Park et al. (2008) and Yang et al. (2020b), this paper uses the  
 134 hierarchical clustering algorithm (HCA) to classify the CS types. The HCA (Rokach et al., 2005) creates  
 135 a hierarchical nested clustering tree by calculating the similarity between different categories of data  
 136 samples. In the clustering tree, the original data samples of different types are at the lowest level of the  
 137 tree, and the top level of the tree is the root point of a cluster. This paper uses Euclidean distance to  
 138 calculate the distance (similarity) between different samples. Here, we introduce the silhouette coefficient  
 139 to determine the best classification number (Rousseeuw, 1987). For any sample  $i$ , the silhouette  
 140 coefficient  $s(i)$  is defined as:

$$141 \quad s(i) = \frac{b(i) - a(i)}{\max\{a(i), b(i)\}} \quad (1)$$

142  $a(i)$  means the average distance from sample  $i$  to all other samples in the cluster it belongs to, and  $b(i)$   
 143 means the lowest average distance from sample  $i$  to all samples in any other cluster. The silhouette  
 144 coefficient of the clustering result is the average of the silhouette coefficients of all samples. The range  
 145 of silhouette coefficient is -1 to 1. The closer to 1, the better the classification results.



146 According to the principle of maximum distance between clusters, the CSs from 1980-2017 can be  
147 classified into two categories (Figure 3a). The silhouette coefficient of the clustering model shows that  
148 when all CSs are divided into two types, the difference between them is the largest. Figures 3c and 3d  
149 show the composite GPH anomalies at 300 hPa that depict the blocking CSs and wave-train CSs. Such  
150 classification results are consistent with previous studies (Park et al., 2014, 2015). The cold air of the  
151 blocking CSs mainly moves in a north-south direction that invades from Siberia to EC, and the cold air  
152 of the wave-train CSs originating from the Ural Mountains converged near Lake Baikal then invaded EC.

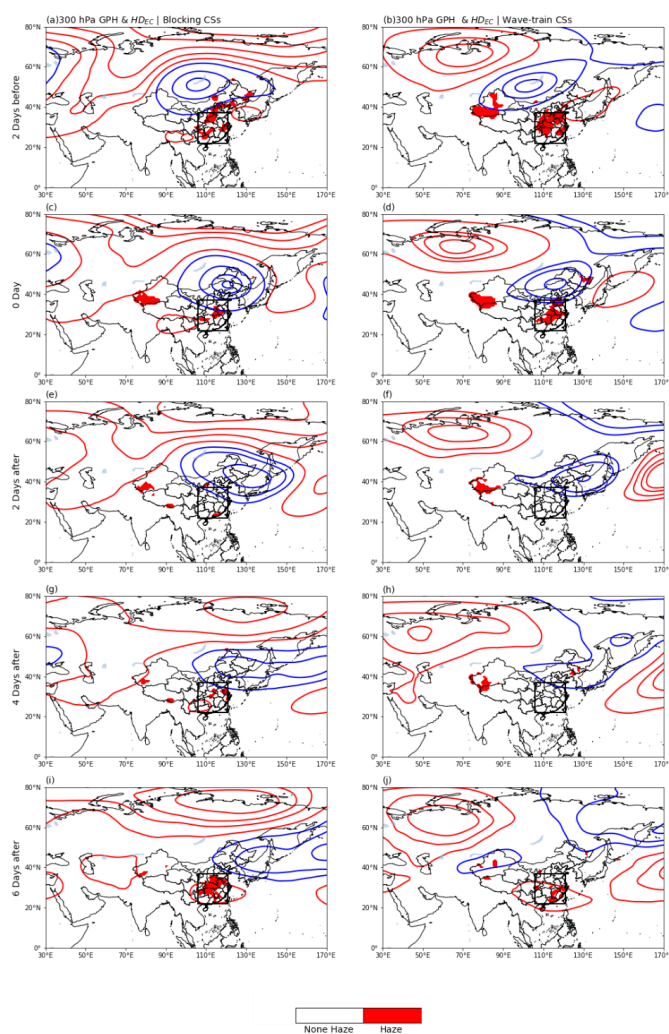


153  
154 **Figure 3.** Hierarchical clustering tree (a) and silhouette coefficient (b) of cool season CSs in the EC. Composite of  
155 GPH anomalies at 300 hPa (shading; gpm) relative to blocking CSs (c) and wave-train CSs (d). Dotted areas are  
156 statistically significant at the 95% confidence level.

157  
158 Figure 4 presents the circulation anomalies from -2 days to 6 days of the CSs events in the two types  
159 and the related evolution of  $HD_{EC}$ . For the blocking CSs, largely positive and negative GPH anomalies  
160 at 300 hPa are found over the Arctic and EC. The  $HD_{EC}$  tends to dissipate first and then increase rapidly  
161 after the CSs erupt. 6 days after the CSs erupt, the haze reaches a relatively large value (Figure 4i). For  
162 the wave-train CSs, a zonal wave-train structure of GPH anomalies can be seen in the midlatitude of the  
163 Eurasian. From -2 days to 6 days, the wave-train with northwest-eastern direction appears to move toward  
164 EC. With the movement of the wave-train, the haze dissipates rapidly, and EC can maintain high air  
165 quality weather for a longer time. Sporadic  $HD_{EC}$  does not appear until 6 days after, which is different



166 from the existence of  $HD_{EC}$  when the blocking CSs occur. It shows that blocking CSs have a weak ability  
167 to dissipate haze compared with wave-train CSs. This conclusion is also consistent with the individual  
168 cases mentioned above. In addition, we also used  $PM_{2.5}$  concentration data (acquired from the China  
169 National Environmental Monitoring Centre and were widely used in the research of  $PM_{2.5}$  in China,  
170 refer to Yin et al. (2021) and Wang et al. (2021)) together with NCEP/NCAR Reanalysis datasets (Kalnay  
171 et al., 1996) to verify the response of  $PM_{2.5}$  to the two types of CSs from 2014 to 2019, and the similar  
172 results were obtained (Figure S2). It shows that the selection of data sets does not affect the main  
173 conclusions of this paper.



174

175 **Figure 4.** Composite of GPH anomalies at 300 hPa (contour; in intervals of 20 gpm) from -2 days to 6 days relative



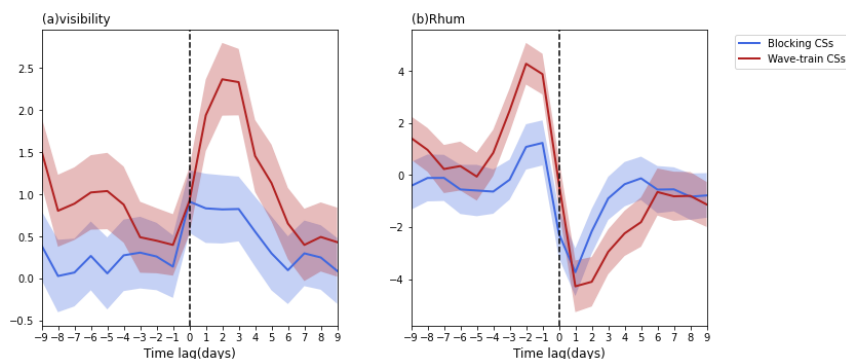


176 to blocking CSs and the corresponding spatial distribution of HD<sub>EC</sub> (shading, only shows the areas which are  
177 statistically significant at the 95% confidence level.) (a, c, e, g, i). b, d, f, h, and j are same as a, c, e, g, and i, but for  
178 wave-train CSs.

179

### 180 3.2 Why are two types of CSs different in dispersing HD<sub>EC</sub>?

181 According to the definition of HD<sub>EC</sub>, which combines visibility and Rhum in this study, we  
182 composite the daily visibility anomalies and Rhum anomalies for 9 days before and after the outbreak of  
183 the blocking CSs and wave-train CSs, respectively (Figure 5). This helps to understand why the two  
184 types of CSs have different abilities to disperse HD<sub>EC</sub>. According to our definition, haze is determined  
185 by visibility and Rhum. Considering two types of CSs, it was found that there is no significant difference  
186 in Rhum between the two kinds of CSs. However, the blocking CSs are generally less effective in  
187 improving visibility than the wave-train CSs. On the day when the blocking CSs outbreak, the visibility  
188 shows a rising trend; however, it begins to deteriorate continuously 3 days after. Though the visibility in  
189 EC has a noticeable downward trend 5 days before the outbreak of the wave-train CSs, it improves  
190 significantly on the day of the wave-train CSs outbreak and rapidly deteriorates again about 3 days after  
191 the wave-train CSs occur. Combined with the differences in the circulation evolution during the two  
192 types of CSs shown in Figure 4, the weak dissipating ability to block CSs during HD<sub>EC</sub> may be related  
193 to the stable blocking anomalies, while the significant cyclical variations of visibility during the wave-  
194 train CSs may be related to the "+-+" wave-train structure anomalies transporting rapidly to the eastern.



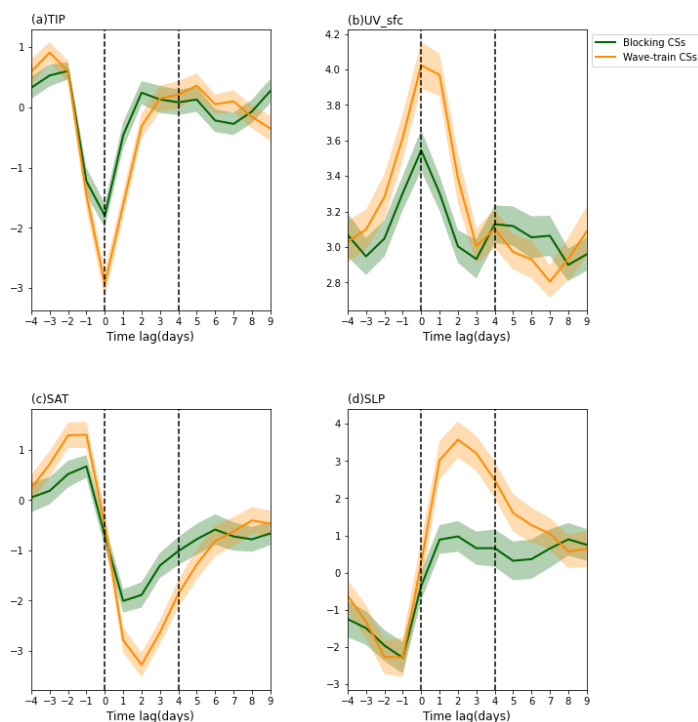
195

196 **Figure 5.** Mean (a) visibility anomalies (km), and (b) Rhum anomalies (%) in EC during 9 days before and after the  
197 outbreak of the blocking CSs (blue lines) and wave-train CSs (red lines), respectively. Shading represents plus/minus  
198 one standard deviation among the CSs.



199  
200 Previous studies show that haze is influenced by surface meteorological conditions (Wang et al.,  
201 2015a; Yin et al., 2019a), which have significant variations after the outbreak of CSs (Park et al., 2014).  
202 Figure 6 reveals the thermal inversion potential anomalies (TIP, defined as the air temperature at 850 hPa  
203 minus SAT referring to Yin et al. (2019b)), surface horizontal wind speed (UV\_sfc) anomalies, SAT  
204 anomalies, and SLP anomalies for 4 days before and after the outbreak of the blocking CSs and wave-  
205 train CSs, respectively. The results show that the high variations of meteorological elements reached the  
206 strongest on the day of the CSs outbreak, and their anomalies weakened in the next 4 days. Compared  
207 with the blocking CSs, the variation of meteorological elements related to wave-train CSs is stronger. 4  
208 days after the outbreak of the two types of CSs, the difference of TIP and UV\_sfc between the two types  
209 of CSs tended to be the same. However, the negative SAT anomalies and the positive SLP anomalies  
210 caused by the wave-train CSs lasted longer than those caused by the blocking CSs. This is in line with  
211 the difference in HD<sub>EC</sub> dispersion ability between the two types of CSs.

212 It should be noted that the SAT and SLP anomalies caused by the two types of CSs in this paper are  
213 different from those of Park et al. (2014). It is due to the regions they selected to identified CSs included  
214 the northern part of Northeast Asia. The invasion of cold air is generally from north to south, so their  
215 research covers more CSs in Northeast Asia, while our study only focuses on CSs in eastern China with  
216 heavy haze. If we choose the same region to identify, similar results can be obtained (Figure S3).



217

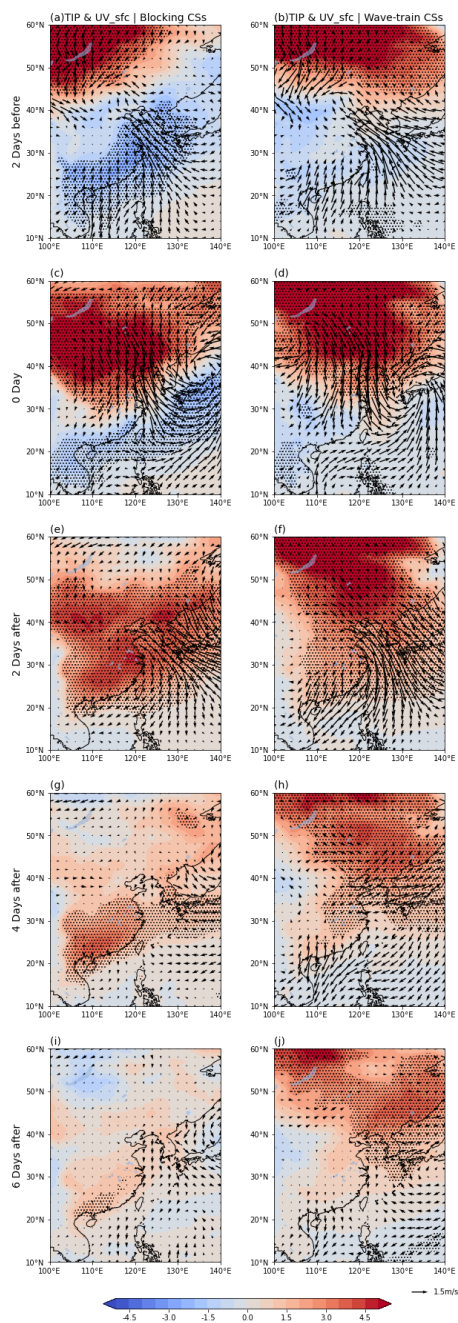
218 **Figure 6.** Mean (a) TIP anomalies (K), (b) UV\_sfc anomalies ( $\text{m s}^{-1}$ ), (c) SAT anomalies (K), and (d) SLP anomalies  
219 (hPa) in EC during 9 days before and after the outbreak of the blocking CSs (blue lines) and wave-train CSs (red  
220 lines), respectively. Shading represents plus/minus one standard deviation among the CSs.

221

222 CSs invade EC would cause a sharp drop in temperature, which may strengthen the TIP in the lower  
223 atmosphere (Lin et al., 2009). The strong TIP is unfavorable for the vertical dispersion of haze, making  
224 the cold, dry, and clear air difficult to spread (Chen et al., 2015; Zhong et al., 2019). Figure 7 indicates  
225 that the cold front will lead the TIP to control EC, forming a conducive condition to HD<sub>EC</sub>, which may  
226 also be a reason for the rapid decline of visibility in EC 2 days after the outbreak of CSs. Compared with  
227 the wave-train CSs, the TIP after the outbreak of blocking CSs maintained for a longer time and a larger  
228 control region, which may cause the weak dispersion ability to HD<sub>EC</sub>. From the perspective of UV\_sfc,  
229 the cold air was limited to the north, and the warm and humid conditions in EC were maintained before  
230 the outbreak of the CSs. The CSs cause the airflow with the northern wind component to invade EC,  
231 rapidly dispersing the haze and causing the visibility to rise. However, after the outbreak of the CSs, the  
232 anomalies of UV\_sfc in EC decrease abnormally, providing conducive conditions to the generation and



233 maintenance of haze. The anomalies of UV\_sfc in EC after the outbreak of blocking CSs are weaker and  
234 have a shorter duration than wave-train CSs.

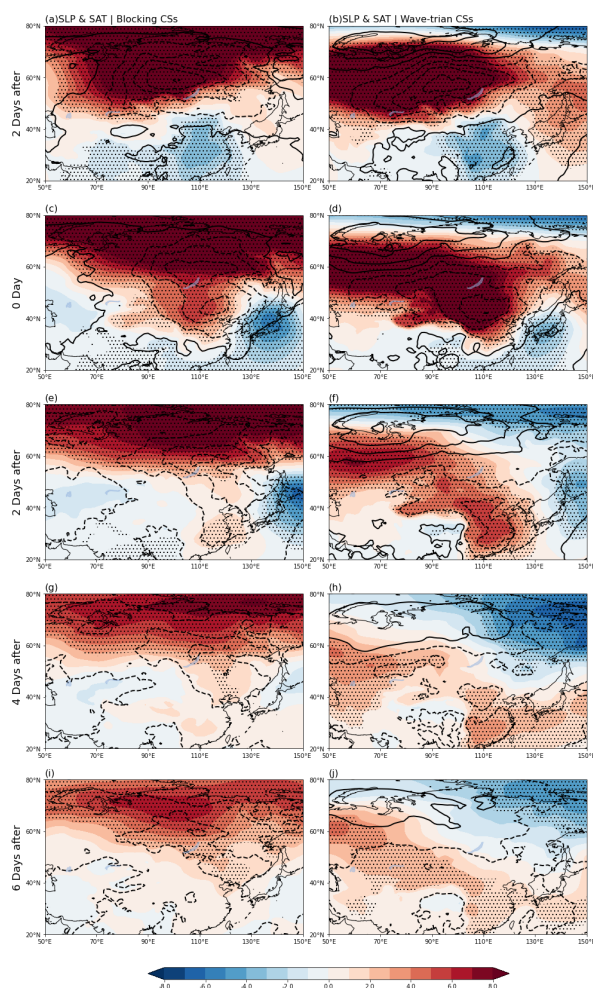


235



236 **Figure 7.** Composite anomalies of TIP (shading; K; dotted areas are statistically significant at the 95% confidence  
237 level) and UV\_sfc (vectors;  $\text{m s}^{-1}$ ) from -2 days to 6 days relative to the outbreak of blocking CSs (a, c, e, g, i) and  
238 the wave-train CSs (b, d, f, h, j).

239 The increase of Siberian high accompanies the outbreak of CSs and the splitting and southward  
240 movement of the Siberian high leads cold air into EC. Comparatively speaking, the distribution of SLP  
241 anomalies in Eurasia before the blocking CSs form a pattern similar to the negative phase of the Arctic  
242 oscillation. Figure 8 shows that when the blocking CSs occur, the positive SLP anomalies and the  
243 negative SAT anomalies in the high-latitudes move southward, and the positive SLP anomalies control  
244 EC. 2 days after the outbreak of the blocking CSs, the positive SLP anomalies, and the negative SAT  
245 anomalies in the EC decline rapidly, providing favorable conditions for the accumulation of pollutants.  
246 The occurrence of wave-train CSs is accompanied by the eastward movement of significant positive SLP  
247 anomalies and negative SAT anomalies. 2 days after, the positive SLP anomalies affect EC continuously,  
248 resulting in a longer period of high visibility in EC.



249

250 **Figure 8.** Composite anomalies of SLP (shading; hPa; dotted areas are statistically significant at the 95% confidence  
251 level) and SAT (contour; K) from -2 days to 6 days relative to the blocking CSs (a, c, e, g, i) and the wave-train CSs  
252 (b, d, f, h, j).

253

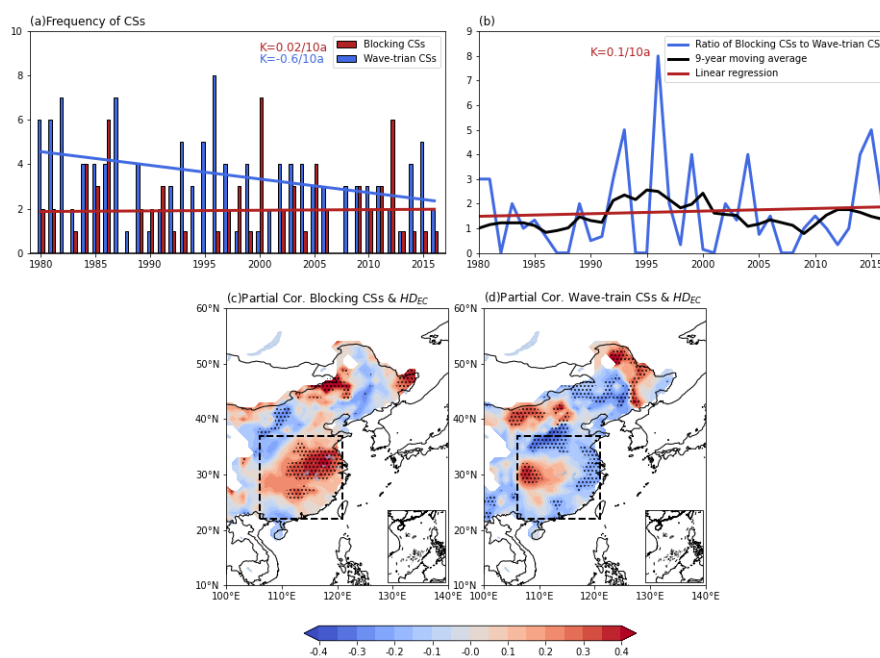
254 The results discussed earlier indicate that the blocking CSs have a weak ability to dissipate the  
255  $HD_{EC}$ , while the outbreak of wave-train CSs can make EC maintain high air quality for a longer time.  
256 Thus, the frequency variations of the two types of CSs may also affect the trend of  $HD_{EC}$  in recent years.  
257 Figure 9a displays the time series of the frequency of blocking CSs and wave-train CSs. The results show  
258 that the wave-train CSs have an obvious downward trend, and the blocking CSs have a slight upward  
259 trend. To get a better sense of the variation of the two types of CSs, the ratio of blocking CSs to wave-



260 train CSs is shown in Figure 9b, which has a visible upward trend, and its 9-year moving average exhibits  
261 a significant interdecadal variation. It means that in recent years, the ability of CSs to dissipate  $HD_{EC}$  has  
262 decreased in general.

263 We further calculated the partial correlation coefficients between the frequency of blocking CSs  
264 (wave-train CSs) and  $HD_{EC}$  to exclude the influence of another type of CSs. It can be found that there is  
265 a significant positive correlation between blocking CSs and  $HD_{EC}$  (Figure 9c). It should be noted that this  
266 does not mean that more blocking CSs cause more haze but reflects the weak dispersion ability of  
267 blocking CSs to  $HD_{EC}$ , resulting in relatively more  $HD_{EC}$ . The negative correlation between wave-train  
268 CSs and  $HD_{EC}$  is significant (Figure 9d), which is consistent with the result above. Furthermore, previous  
269 studies have shown that with the appearance of a warm Arctic-cold Eurasian pattern, there will be more  
270 blocking high maintained in the winter (Cohen et al., 2014; Luo et al., 2016), causing more blocking CSs  
271 to invade East Asia, and the phenomenon is further intensified under global warming (Yang et al., 2020b).  
272 It can be considered that ability of CSs to dissipate haze in East Asia weakened in the future, and  
273 policymakers are required to consider the problem of air pollutions.

274



275

276 **Figure 9.** (a) Time series of the blocking CSs and the wave-train CSs (The solid line is the linear regression of the  
277 time series, and the text in the upper right corner indicates the trend of the solid lines). (b) Time series of the ratio of



278 blocking CSs to wave-train CSs (blue), 9-year moving average (black), and linear regression (red). The partial  
279 correlation coefficient between  $HD_{EC}$  and the frequency of blocking CSs (c) and the wave-train CSs (d). Dotted areas  
280 are statistically significant at the 95% confidence level.

#### 281 4. Conclusions and discussion

282 In this paper, the connection between the CSs and the cool season haze over the EC is investigated  
283 based on the observational and reanalysis datasets from 1980 to 2017. The 187 CSs over EC are classified  
284 into two types by HCA, blocking CSs and wave-train CSs. Usually, the blocking CSs are accompanied  
285 by a meridional dipole in the upper-tropospheric GPH anomalies, which consists of a stable blocking  
286 structure. The blocking structure tends to control the EC for a long time and forms a relatively stable  
287 meteorological condition, which has the disadvantage to dissipate the  $HD_{EC}$ . Correspondingly, the local  
288 meteorological conditions, especially TIP and the quiescent wind band, rapidly appear after the blocking  
289 CSs outbreak, provide a haze-prone background. In addition, the positive SLP anomalies induced by the  
290 outbreak of the blocking CSs can rapidly restore to normal, and the SAT warm up under the influence of  
291 the weakening of the north wind component. Therefore, the ability to block CSs to dissipate  $HD_{EC}$  is  
292 limited. On the contrary, high air quality in EC can last longer due to the shorter duration of TIP and  
293 longer duration of positive SLP anomalies. In general,  $HD_{EC}$  can remain at a low level for a shorter  
294 (longer) time after the outbreak of blocking (wave-train) CSs. It is confirmed that blocking CSs has been  
295 increased over the past few years (Park et al., 2011a; Luo et al., 2018). Furthermore, the increasing trend  
296 of blocking CSs is likely to continue in the future, which may weaken the dispersion of haze and worsen  
297 the  $HD_{EC}$ . This reminds us that the problem of air pollution is still very serious and needs more attention.

298 Finally, it should be noted that the lack of meteorological station information in the observed data  
299 limits the accuracy of the haze distribution to some extent. Previous studies documented that the CSs  
300 outbreak greatly affected the dispersion of haze (Lin et al., 2009 and Wang et al., 2016). However, it can  
301 be seen that the visibility anomalies from -5 days to the day of the wave-train CSs outbreak have a sharp  
302 decline trend. Whether the CSs aggravate the haze before the outbreak deserves our attention in future  
303 research. In addition, to better understand the formation of haze and improve the predictability of haze,  
304 more research is needed to explore the possible impacts of meteorological elements on haze pollution in  
305 China.





306

307 **Data availability**

308 The ground observations are from the website: <http://data.cma.cn>. Daily mean meteorological data  
309 are obtained from the ERA-Interim reanalysis data archive: [http://www.ecmwf.int/en/research/climate-](http://www.ecmwf.int/en/research/climate-reanalysis/era-interim)  
310 [reanalysis/era-interim](http://www.ecmwf.int/en/research/climate-reanalysis/era-interim).

311 **Author contributions**

312 SZ and GZ put forward the idea and design research, RW provided observational data including  
313 relative humidity, visibility, and weather phenomena. SZ and XY performed research, and ZY provided  
314 valuable suggestions. SZ wrote the manuscript with contributions from all co-authors.

315 **Competing interests**

316 The authors declare that they have no conflict of interest.

317 **Acknowledgements**

318 This research is supported by the National Key Research and Development Program of China  
319 (2017YFA0603804) and the National Natural Science Foundation of China (41575085).

320 **References**

321 Ashfold, M. J., Latif, M. T., Samah, A. A., Mead, M. I., Harris, N. R. P.: Influence of Northeast Monsoon  
322 cold surges on air quality in Eastern Asia, *Atmospheric Environment*, 166, 498-509,  
323 <https://doi.org/10.1016/j.atmosenv.2017.07.047>, 2017.

324 Cai, B., Zeng, G., Zhang, G. and Li, Z.: Autumn cold surge paths over North China and the associated  
325 atmospheric circulation, *Atmosphere*, 10, 134, <https://doi.org/10.3390/atmos10030134>, 2019.

326 Cai, W. J., Li, K., Liao, H., Wang, H. J., and Wu, L. X.: Weather Conditions Conducive to Beijing Severe  
327 Haze More Frequent under Climate Change, *Nat. Clim. Change*, 7, 257–262,  
328 <https://doi.org/10.1038/nclimate3249>, 2017.



- 329 CCiM, G.R.: The horizontal and vertical structure of East Asia winter monsoon pressure surges, QJR  
330 Meteorol. Soc, 125, 29–54, <https://doi.org/10.1002/qj.49712555304>, 1999.
- 331 Chai, D. H., Wu, M. H., Li, J. X., Zhao, Y. Q.: Analysis of greenhouse effect of cold wave low temperature  
332 on different structures in 2000 (in Chinese), Meteorological Science, 2002(03), 367-371, 2002.
- 333 Chang, L. Y., Xu, J. M., Tie, X. X., and Wu, J. B.: Impact of the 2015 El Nino event on winter air quality  
334 in China, Sci. Rep., 6, 34275, <https://doi.org/10.1038/srep34275>, 2016.
- 335 Chen, H. P., Wang, H.J.: Haze Days in North China and the associated atmospheric circulations based on  
336 daily visibility data from 1960 to 2012, Journal of Geophysical Research: Atmospheres, 120(12), 5895–  
337 5909, <https://doi.org/10.1002/2015JD023225>, 2015.
- 338 Cohen, J., Screen, J., Furtado, J., et al.: Recent Arctic amplification and extreme mid-latitude weather,  
339 Nature Geoscience, 7, 627–637. <https://doi.org/10.1038/ngeo2234>, 2014.
- 340 Compo, G. P., Kiladis, G. N., and Webster, P. J.: The horizontal and vertical structure of east Asian winter  
341 monsoon pressure surges, Q. J. R. Meteorol. Soc., 125, 29–54,  
342 <https://doi.org/10.1002/qj.49712555304>, 1999.
- 343 Dee, D., and Coauthors.: The ERA-interim reanalysis: configuration and performance of the data  
344 assimilation system, Quarterly Journal of the Royal Meteorological Society, 137, 553–597,  
345 <https://doi.org/10.1002/qj.828>, 2011.
- 346 Ding, Y. H., and Liu, Y. J.: Analysis of long-term variations of fog and haze in China in recent 50 years  
347 and their relations with atmospheric humidity, Sci. China Ser. D: Earth Sci., 57, 36–46,  
348 <https://doi.org/10.1007/s11430-013-4792-1>, 2014.
- 349 Fu, C. B., Wu, J., Gao, Y. C., Zhao, D. M., Han, Z.W.: ConECutive extreme visibility events in China  
350 during 1960–2009, Atmos. Environ., 68, 1–7, <https://doi.org/10.1016/j.atmosenv.2012.11.035>, 2013.
- 351 Han, S. Q., Bian, H., Tie, X., Xie, Y., Sun, M., Liu, A.: Impact measurements of nocturnal planetary  
352 boundary layer on urban air pollutants: From a 250-m tower over Tianjin, China. J. Hazard. Mater., 162,  
353 264–269, 2009.
- 354 Hien, P.D., Loc, P.D., Dao, N.V.: Air pollution episodes associated with East Asian winter monsoons, Sci.  
355 Total. Environ, 409, 5063–5068, <https://doi.org/10.1016/j.scitotenv.2011.08.049>, 2011.
- 356 Hu, Z.Z., Bengtsson, L., Arpe, K.: Impact of global warming on the Asian winter monsoon in a coupled  
357 GCM, J. Geophys. Res., 05, 4607–4624, <https://doi.org/10.1029/1999JD901031>, 2000.
- 358 Kalnay, E., Kanamitsu, M., Kistler, R., Collins, W., Deaven, D., Gandin, L., Iredell, M., Saha, S., White,



- 359 G., Woollen, J., Zhu, Y., Leetmaa, A., Reynolds, R., Chelliah, M., Ebisuzaki, W., Higgins, W., Janowiak,  
360 J., Mo, K. C., Ropelewski, C., Wang, J., Jenne, R., and Joseph, D.: The NCEP/NCAR 40-year reanalysis  
361 project, *B. Am. Meteorol. Soc.*, 77, 437–471, [https://doi.org/10.1175/1520-](https://doi.org/10.1175/1520-0477(1996)077<0437:TNYRP>2.0.CO;2)  
362 [0477\(1996\)077<0437:TNYRP>2.0.CO;2](https://doi.org/10.1175/1520-0477(1996)077<0437:TNYRP>2.0.CO;2), 1996.
- 363 Lin, C. Y., Lung, S. C. C., Guo, H. R. et al.: Climate variability of cold surge and its impact on the air  
364 quality of Taiwan, *Climatic Change* 94, 457–471, <https://doi.org/10.1007/s10584-008-9495-9>, 2009.
- 365 Luo, D. H., Chen, X. D., Dai, A. G et al.: Changes in Atmospheric Blocking Circulations Linked with  
366 Winter Arctic Warming: A New Perspective, *Journal of Climate*, 31 (18), 7661–7678,  
367 <https://doi.org/10.1175/JCLI-D-18-0040.1>, 2018.
- 368 Luo, D. H., Xiao, Y. Q., Yao, Y., Dai, A. G. et al.: Impact of Ural Blocking on Winter Warm Arctic–Cold  
369 Eurasian Anomalies. Part I: Blocking-Induced Amplification, *Journal of Climate*, 29 (11), 3925–3947,  
370 <https://doi.org/10.1175/JCLI-D-15-0611.1>, 2016.
- 371 Luo, Y. F., Lu, D., Zhou, X. J.; Li, W. L.: Characteristics of the spatial distribution and yearly variation  
372 of aerosol optical depth over China in last 30 years, *J. Geophys. Res.*, 106(D13), 14,501–14,513,  
373 <https://doi.org/10.1029/2001JD900030>, 2001.
- 374 Niu, F., Li, Z. Q., Li, C., Lee, K.-H., Wang, M. Y.: Increase of wintertime fog in China: Potential impacts  
375 of weakening of the eastern Asian monsoon circulation and increasing aerosol loading, *J. Geophys. Res.*,  
376 115, D00K20, <https://doi.org/10.1029/2009JD013484>, 2010.
- 377 Park, T. W., Ho, C. H., Jeong, J. H., et al.: Different characteristics of cold day and cold surge frequency  
378 over East Asia in a global warming situation, *Journal of Geophysical Research: Atmospheres*,  
379 116(D12), D12118, <https://doi.org/10.1029/2010JD015369>, 2011a.
- 380 Park, T. W., Ho, C. H., Yang, S.: Relationship between the Arctic Oscillation and Cold Surges over East  
381 Asia, *J. Clim.*, 24(1), 68–83, <https://doi.org/10.1175/2010jcli3529.1>, 2011b.
- 382 Park, T. W., Jeong, J. H., Ho, C. H., et al.: Characteristics of atmospheric circulation associated with cold  
383 surge occurrences in East Asia: A case study during 2005/06 winter, *Adv. Atmos. Sci.*, 25, 791–804,  
384 <https://doi.org/10.1007/s00376-008-0791-0>, 2008.
- 385 Park, T. W., Ho, C. H., Jeong, J. H., et al.: A new dynamical index for classification of cold surge types over  
386 East Asia, *Climate dynamics*, 45(9): 2469–2484, <https://doi.org/10.1007/s00382-015-2483-7>, 2015.
- 387 Park, T. W., Ho, C. H., Deng, Y.: A synoptic and dynamical characterization of wave-train and blocking  
388 cold surge over East Asia, *Clim Dyn* 43, 753–770, <https://doi.org/10.1007/s00382-013-1817-6>, 2014.



- 389 Qian, Y., Leung, L. R., Ghan, S. J. Giorgi, F.: Regional climate effects of aerosols over China: Modeling  
390 and observation, *Tellus*, 55B, 914–934, <https://doi.org/10.3402/tellusb.v55i4.16379>, 2003.
- 391 Qu, W., Wang, J., Zhang, X., Yang, Z., Gao, S.: Effect of cold wave on winter visibility over eastern  
392 China, *J. Geophys. Res.*, 120, 2394–2406, <https://doi.org/10.1002/2014JD021958>, 2015.
- 393 Rokach, L., Maimon, O.: Clustering methods. *Data mining and knowledge discovery handbook*, Springer  
394 US, 321-352, 2005.
- 395 Rousseeuw, P.: Silhouettes: A graphical aid to the interpretation and validation of cluster analysis. *Journal*  
396 *of Computational and Applied Mathematics*, 20, 5365, [https://doi.org/10.1016/0377-0427\(87\)90125-](https://doi.org/10.1016/0377-0427(87)90125-7)  
397 [7](https://doi.org/10.1016/0377-0427(87)90125-7), 1987.
- 398 Shi, C., Zhang, H., Roth, M., Li, Z.: Impacts of urbanization on long-term fog variation in Anhui Province,  
399 China. *Atmos. Environ.*, 42, 8484–8492, <https://doi.org/10.1016/j.atmosenv.2008.08.002>, 2008.
- 400 Wang, H. J., and Chen, H. P.: Understanding the recent trend of haze pollution in eastern China: roles of  
401 climate change, *Atmos. Chem. Phys.*, 16, 4205–4211, <https://doi.org/10.5194/acp-16-4205-2016>, 2016.
- 402 Wang, H. J., Chen, H. P., Liu, J. P.: Arctic Sea Ice Decline Intensified Haze Pollution in Eastern China,  
403 *Atmospheric and Oceanic Science Letters*, 8:1, 1-9, <https://doi.org/10.3878/AOSL20140081>, 2015.
- 404 Wang, X, Zhang, R, Tan, Y, et al.: Dominant synoptic patterns associated with the decay process of PM  
405 2.5 pollution episodes around Beijing, *Atmospheric Chemistry and Physics*, 21(4): 2491-2508,  
406 <https://doi.org/10.5194/acp-21-2491-2021>, 2021.
- 407 Wang, Z. S., Liu, X. D., Xie, X. N.: Effects of Strong East Asian Cold Surges on Improving the Air  
408 Quality over Mainland China, *Atmosphere*, 7, 38, <https://doi.org/10.3390/atmos7030038>, 2016.
- 409 Wang, Z., and Ding, Y.: Climate change of the cold wave frequency of China in the last 53 years and the  
410 possible reasons (in Chinese). *Chin. J. Atmos. Sci.*, 30, 1068–1076, 2006.
- 411 Wei, Y., Li, J., Wang, Z., Chem, H., Wu, Q., Li, J., Wang, Y., and Wang, W.: Trends of surface PM<sub>2.5</sub>  
412 over Beijing–Tianjin–Hebei in 2013–2015 and their causes: emission controls vs. meteorological  
413 conditions, *Atmos. Oceanic Sci. Lett.*, 10, 276–283, <https://doi.org/10.1080/16742834.2017.1315631>,  
414 2017.
- 415 Wu, J., Fu, C. B., Zhang, L. Y., Tang, J. P.: Trends of visibility on sunny days in China in the recent 50  
416 years, *Atmos. Environ.*, 55, 339–342, <https://doi.org/10.1016/j.atmosenv.2012.03.037>, 2012.
- 417 Wu, J., Luo, J. G., Zhang, L. Y., Xia, L., Zhao, D. M., Tang, J. P.: Improvement of aerosol optical depth  
418 retrieval using visibility data in China during the past 50 years, *J. Geophys. Res. Atmos.*, 119, 13,370–



- 419 13,387, <https://doi.org/10.1002/2014JD021550>, 2014.
- 420 Xie, Y. B., Chen, J., and Li, W.: An assessment of PM<sub>2.5</sub> related health risks and impaired values of  
421 Beijing residents in a consecutive high-level exposure during heavy haze days, *Environ. Sci.*, 35, 1–8,  
422 2014.
- 423 Xu, P., Chen, Y. F., and Ye, X. J.: Haze, air pollution, and health in China, *Lancet*, 382, 2067,  
424 [https://doi.org/10.1016/S0140-6736\(13\)62693-8](https://doi.org/10.1016/S0140-6736(13)62693-8), 2013.
- 425 Xu, Q.: Abrupt change of themid-summer climate in central east China by the influence of atmospheric  
426 pollution, *Atmos. Environ.*, 35, 5029–5040, [https://doi.org/10.1016/S1352-2310\(01\)00315-6](https://doi.org/10.1016/S1352-2310(01)00315-6), 2001.
- 427 Yang, X. Y., Zeng, G., Zhang, G. W., Li, Z.X.: Interdecadal Variation of Winter Cold Surge Path in East  
428 Asia and Its Relationship with Arctic Sea Ice, *Journal of Climate*, 33(11), 4907–4925,  
429 <https://doi.org/10.1175/JCLI-D-19-0751.1>, 2020a.
- 430 Yang, X. Y., Zeng, G., Zhang, G. W., Vedaste, I., Xu, Y.: Future projections of winter cold surge paths  
431 over East Asia from CMIP6 models, *International Journal of Climatology*, 1–16,  
432 <https://doi.org/10.1002/joc.6797>, 2020b.
- 433 Yin, Z, Zhang, Y, Wang, H, et al.: Evident PM 2.5 drops in the east of China due to the COVID-19  
434 quarantine measures in February, *Atmospheric Chemistry and Physics*, 21(3): 1581–1592,  
435 <https://doi.org/10.5194/acp-21-1581-2021>, 2021.
- 436 Yin, Z. C., Wang, H. J.: Possible Relationship between the Chukchi Sea Ice in the Early Winter and the  
437 February Haze Pollution in the North China Plain., 32(16), 5179–5190, [https://doi.org/10.1175/JCLI-](https://doi.org/10.1175/JCLI-D-18-0634.1)  
438 [D-18-0634.1](https://doi.org/10.1175/JCLI-D-18-0634.1), 2019b.
- 439 Yin, Z.C., Li, Y. Y., Wang, H. J.: Response of early winter haze in the North China Plain to autumn  
440 Beaufort sea ice, *Atmos. Chem. Phys.*, 19, 1439–1453, <https://doi.org/10.5194/acp-19-1439-2019>,  
441 2019a.
- 442 Yin, Z.C., Wang, H.J., and Chen, H. P.: Understanding severe winter haze events in the North China  
443 Plain in 2014: Roles of climate anomalies, *Atmos. Chem. Phys.*, 17, 1641–1651,  
444 <https://doi.org/10.5194/acp-17-1641-2017>, 2017.
- 445 Zhang, L. Y., Lu, X. B., Yang, L. L., Ding, F., Zhu, Z. F., and Rui, D. M.: Study on the Effects of the  
446 Strong El Nino Event on Air Quality of Eastern China in Winter, *The Administration and Technique of*  
447 *Environmental Monitoring*, 28, 23–27, 2016.
- 448 Zhong, W. G., Yin, Z. C., Wang, H. J.: The relationship between anticyclonic anomalies in northeastern



- 449 Asia and severe haze in the Beijing–Tianjin–Hebei region, Atmos. Chem. Phys., 19, 5941–5957,  
450 <https://doi.org/10.5194/acp-19-5941-2019>, 2019.